Efficient Two-Dimensional Defect-Free Dual-Species Atom Arrays Rearrangement Algorithm with Near-Fewest Atom Moves

Zhi-Jin Tao(陶知进)[1,2†], Li-Geng Yu(余立庚)[1,2†], Peng Xu(许鹏)[1,3*], Jia-Yi Hou(侯嘉毅)[1], Xiao-Dong He(何晓东)[1], and Ming-Sheng Zhan(詹明生)[1,3]

[1]*State Key Laboratory of Magnetic Resonance and Atomic and Molecular Physics, Wuhan Institute of Physics and Mathematics, Innovation Academy for Precision Measurement Science and Technology, Chinese Academy of Sciences, Wuhan 430071, China*
[2]*School of Physics and Technology, Wuhan University, Wuhan 430072, China*
[3]*Wuhan Institute of Quantum Technology, Wuhan 430206, China*

(Received 19 April 2022; accepted manuscript online 29 June 2022)

Dual-species single-atom array in optical tweezers has several advantages over the single-species atom array as a platform for quantum computing and quantum simulation. Thus, creating the defect-free dual-species single-atom array with atom numbers over hundreds is essential. As recent experiments demonstrated, one of the main difficulties lies in designing an efficient algorithm to rearrange the stochastically loaded dual-species atoms arrays into arbitrary demanded configurations. We propose a heuristic connectivity optimization algorithm to provide the near-fewest number of atom moves. Our algorithm introduces the concept of using articulation points in an undirected graph to optimize connectivity as a critical consideration for arranging the atom moving paths. Tested in array size of hundreds atoms and various configurations, our algorithm shows a high success rate ($> 97\%$), low extra atom moves ratio, good scalability, and flexibility. Furthermore, we propose a complementary step to solve the problem of atom loss during the rearrangement.

DOI: 10.1088/0256-307X/39/8/083701

In the physical implementation of quantum computation, neutral atom array has become a promising candidate for its various and controllable atom-atom interactions (like the van der Wass interaction and Rydberg–Rydberg interaction) and good scalability.[1–4] With the demonstration of high fidelity single qubit gates,[5] entangled states preparation and measurement,[5–8] as well as the CNOT gate demonstration,[9] neutral atom array system has come to a stage of realizing quantum error correction(QEC). In this phase, the mixed-species qubit system is more advantageous than the single species qubit setup with the requirements for simultaneously gate operating and state detecting.[10,11] Especially, the checker board dual-atom configuration in a square optical lattice is a promising platform for implementing large scale quantum error correction based on surface code, because of the reduced cross-talk when implementing the quantum gate and measuring, due to the large resonant frequency difference between the different kinds of atoms.[12]

In the field of quantum simulation, Rydberg atom array serves as an excellent platform to simulate the quantum dynamic model and optimization problems mapped into the Ising model and so on by controlling the interactions between atoms.[13,14] With the dual-species system realized, more types of interactions can be realized, which provides the feasibility to investigate new phenomenons. Also, building single molecules by merging two single atoms has been achieved by different scientific groups recently.[15–18] Thus, the dual-species atom array can also be utilized to construct an atom-molecule system by manipulating two kinds of atoms.

To bring the proposed schemes into practice, preparing an arbitrary user-defined atom array composed of multi-species atoms is indispensable. In the experiment, one of the feasible ways is to prepare many optical traps nearly half fulfilled after initial loading, then rearrange single atoms one by one using movable tweezers to achieve the desired atom array configuration.[19] In this protocol, one of the most intractable obstacles is to develop an algorithm to output an optimized moving path when inputting an initial atom configuration. In the case of single species, there are several efficient and scalable algorithms, including HHA, HPFA, and Hungarian matching.[20–23] As a result, the single-species atom array has been scaled to hundreds of atoms and from one dimension to three dimensions.[24–27] For the defect-free multi-species atom array, there are mainly two experimental routes. One is to build two setups of different wavelengths for separate species, including trap arrays and moving tweezers. In this way, atoms of different species will be stochastically loaded into the traps of corresponding wavelength.[28,29] This route can directly use the extension of single species algorithms[20–23] for many geometries but suffers from more complicated experimental setups, thus has not demonstrated defect-free atom arrays. The other way is to use the identical trap array and moving tweezer for two species. Using the 808-nm tweezer array, Sheng *et al.* have realized defect-free two-dimensional 6×4 dual-species atom assembly of ^{85}Rb (^{87}Rb) atoms with a

†Z. J. Tao and L. G. Yu contributed equally to this work.
*Corresponding authors. Email: xupeng@apm.ac.cn
© 2022 Chinese Physical Society and IOP Publishing Ltd

filling fraction of 0.88 (0.89).[19] However, due to the more complicated situation that the target sites may be filled with unmatched atoms and different types of atoms will block each other in the moving path, the preliminary algorithm demonstrated in the work of Sheng *et al.*[19] is facing a limitation that the success probability decays exponentially with the increasing number of atoms.

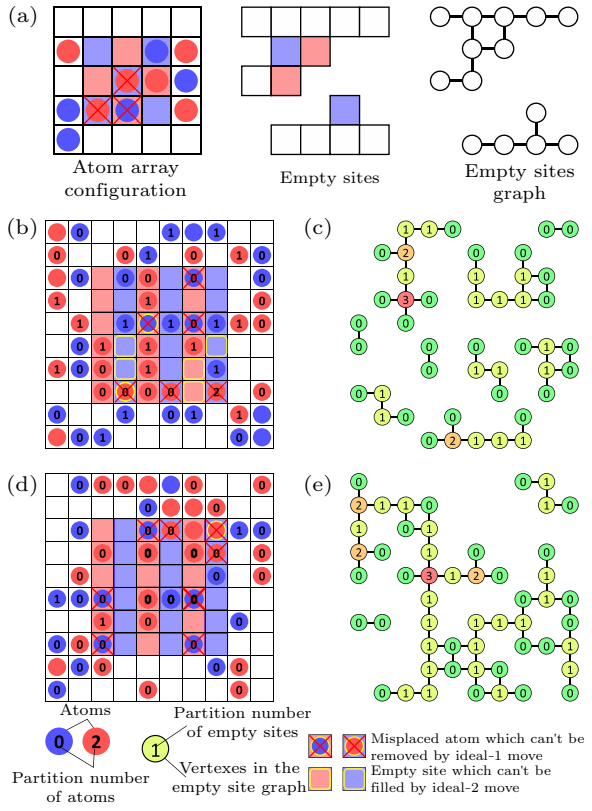

Fig. 1. Examples of dual-species atom arrays and the corresponding empty-site graphs. For schemes of atom arrays, the red (blue) disks denote the single atoms of ^{87}Rb (^{85}Rb), the red(blue)-colored blocks denote the target site of ^{87}Rb (^{85}Rb). For schemes of corresponding empty site graphs, circles denote vertexes, and lines denote edges. Numbers on atoms and empty sites denote the partition number (non-movable atoms have no partition number). (a) Scheme of extracting empty site graphs from atom arrays. (b) An example of atom array after initial stochastic loading. (c) Corresponding empty site graph for (b). (d) Another example of dual-species atom array, whose number of isolated empty site regions is greatly reduced. (e) Corresponding empty site graph for (d).

To provide an efficient, well-optimized, and widely applicable algorithm for mixed-species atom rearrangement, here we propose heuristic connectivity optimized algorithm (HCOA). This algorithm can solve the limitation of the success rate in the second route, and can also be applied to the first route. HCOA is based on the undirected graph which is mapped from dual-species atom distributions. By taking the connectivity of the graph as a critical consideration at the main steps, the success rate of HCOA decreases linearly with the increasing number of atoms and remains larger than 0.80 as the number of target atoms increases up to 3600. To trap more atoms under actual experimental conditions, the algorithm sets that an atom can only be transported along the lattice links.[19–26] Moreover, recent experimental research[22,23,25] has imposed several constraints. First, the algorithm should run in milliseconds magnitude for hundreds of atoms to minimize the total assembly time. Second, the algorithm should reduce the number of atom moves firstly and then shorten the total transport path, because capturing and releasing an atom at the beginning and the end of transport process cost relatively longer time and have limited success rate. Thus, we should reduce the number of atom moves in priority to reach a high experimental success rate.

We start the analysis from one single atom move to approach the near-fewest atom moves. Each single atom move can be decomposed into two parts. The first part is to choose one atom to move, while the second part is to choose an empty site for the chosen atom. After initial stochastic loading, three types of atom-site pairs appear in the atom array. They are misplaced atoms in the wrong sites, atoms in the suitable sites, and outside atoms which do not lie in the target region. As for the empty sites, we classify them into two types, the empty target sites, and the empty outside sites. Totally, there are six types of atom moves according to the classification. Only two types are not redundant and even necessary to achieve the fewest atom moves. One type is moving a misplaced atom to a matched empty target site, which can decrease the number of misplaced atoms and empty target sites. The other type is moving an outside atom to a target empty site to reduce the number of empty target sites. We call the two types of moves the ideal moves and they refer to the first type as ideal-1 move while the latter as ideal-2 move.

After initial stochastic loading, like Fig. 1(b), there are a lot of isolated connected empty site regions, which makes empty sites have fewer atoms to choose from, same as misplaced atoms. On the contrary, the number of ideal moves will increase if the number of isolated, empty site regions becomes less, as shown in Fig. 1(d). Therefore, we can try to merge the isolated, empty site regions as much as possible to improve the connectivity of entire empty site regions in each atom move.

We abstract all the empty sites as an undirected graph $G\langle V, E\rangle$. The vertex set V consists of all empty sites. As for the edge set E, for empty sites $i, j \in V$, if an atom can be transported from site i to j safely, then the tuple $(i, j) \in E$. The isolated, empty site region is equivalent to the concept of the connected component in graph theory. See Fig. 1(a) for a simple example of mapping the empty sites to an undirected graph. To analyze how the number of connected components changes, a new concept called partition number is introduced. The partition number of an atom a for a graph G, denoted as $P(G, a)$, is defined as the reduction number of connected components of the graph G if we treat the atom which is movable as an empty site and add the empty site and its connected edges to the empty site graph G. Furthermore, non-movable atoms have no partition number. The partition number of an empty site s for a graph G, denoted as $P(G, s)$ is defined as the increment number of the connected components if the empty site s and its connected edges are deleted from the graph G. Figures 1(b)–1(d) illustrate

the concept of the partition number. From the definition, in each atom move, to reduce the connected components and improve the graph's connectivity, we can consider as follows. In choosing which atom to move, we can choose the atom with a larger partition number and then update the graph. In choosing empty sites to move the chosen atom into, we should choose the empty sites with the minimum partition number. Then, the graph's connectivity will get improved after such a move. In the Supplementary Materials, we introduced the concept of *branch factor* to prove the effectiveness of improving the connectivity of the graph.

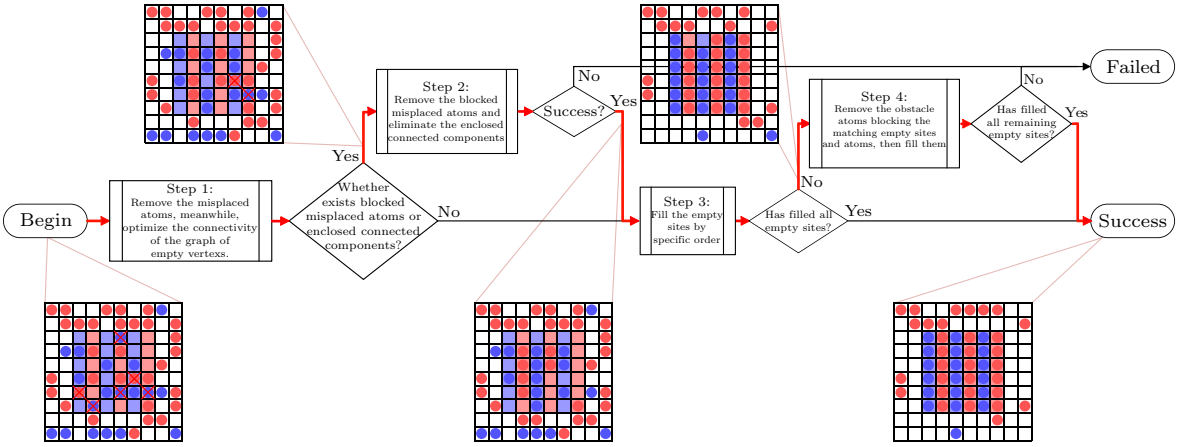

Fig. 2. The brief flowchart of HCOA, with an example of how HCOA processes a stochastically loaded atom array.

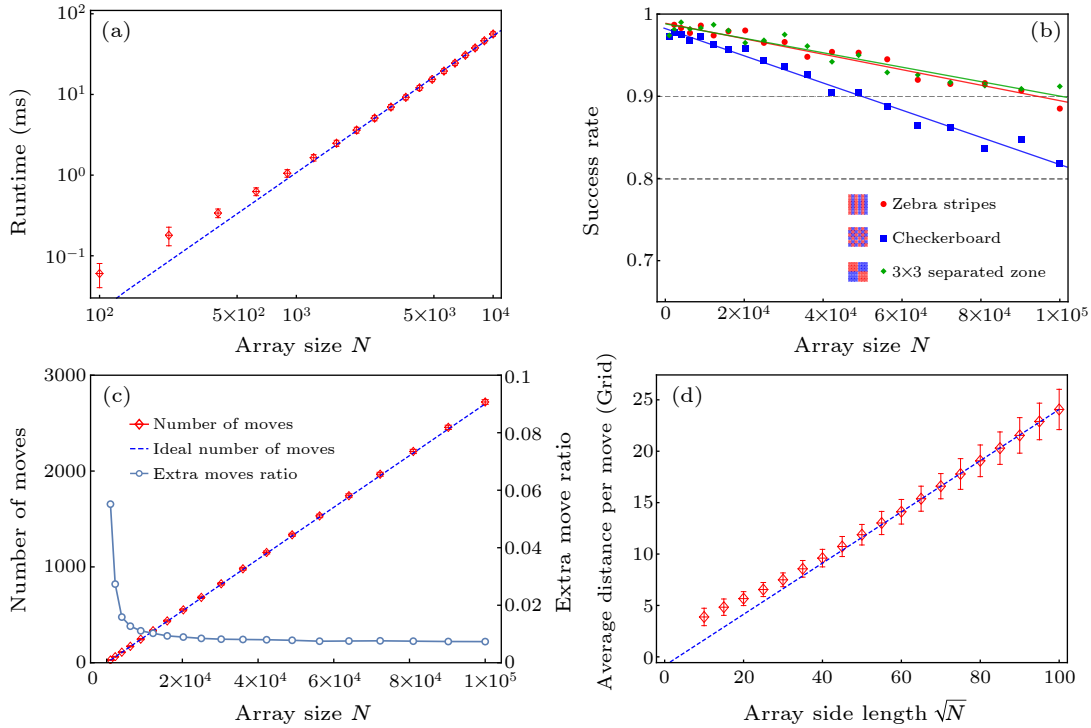

Fig. 3. Simulation results. The errorbars in (a) and (c)–(d) represent the standard deviation. (a) Runtime of HCOA versus array size (zebra stripes pattern). The dashed line is the linear fitting of the last 13 data, having slope 1.70 ± 0.02. (b) Success rate of different patterns versus array size. The success rate of HCOA algorithm is fitted with a linear curve $y = a - bx$, for Zebra strips pattern $a = 0.989 \pm 0.003$, $b = (9.4 \pm 0.6) \times 10^{-6}$, for Checkerboard pattern $a = 0.982 \pm 0.003$, $b = (16.5 \pm 0.5) \times 10^{-6}$ and for 3×3 separated zone $a = 0.988 \pm 0.003$, $b = (8.8 \pm 0.6) \times 10^{-6}$. (c) Number of moves, ideal number of moves and extra move ratio versus array size (zebra strips pattern). (d) Average distance per move versus array side length (zebra stripes pattern). The dashed line is the linear fitting of the last 9 data.

Based on the above analysis, the general steps of our algorithm are as follows: (1) Move the misplaced atoms to the appropriate empty sites directly (i.e., make the ideal-1 moves as more as possible), and the partition number will be taken as an essential consideration. (2) Remove the misplaced atoms left unsolved by step 1 and let all target empty site regions connected with the outside by moving matched atoms in the target region. (3) Fill the empty tar-

get sites with the matched outside atoms (i.e., make the ideal-2 moves). (4) Solve the most common unsolved cases left by step 3. The brief flowchart is in Fig. 2. The details of each step are stated in the Supplementary Materials.

Our algorithm is used for the array of hundreds of atoms and different configurations, as shown in Fig. 3. The runtime data is performed with a C++ code with gcc compiler opening -O3 optimization and an AMD CPU Ryzen 7 5700U. Three target array pattern "Zebra Stripes", "Checkerboard" or "3×3 separated zone" are respectively tessellation of $1\times N_{\rm T}^{1/2}$, 1×1 or 3×3 block of the two different species atoms (as demonstrated in Ref. [19]). The target region with the size of $N_{\rm T}/N=0.36$ is located at the center of the trap array, where $N_{\rm T}$ is the number of target sites. Each data is tested 1000 times. Without special instruction, the loading ratio is 0.5, and the ratio between the two species is 1 : 1. The runtime curve [see Fig. 3(a)] shows that the time complexity of the algorithm is approximately $O(N^2)$. The runtime of HCOA is less than 1 ms for intermediate-scale array ($N<700$) and around 60 ms for 100×100 atom array with 60×60 target array, showing that HCOA is efficient enough for current and near-future dual-species atom array preparation experiment. More importantly, the success rate of HCOA decreases linear with the number of atoms increasing [see Fig. 3(b)], which is high (>0.97) for intermediate-scale arrays and remains at a high level (>0.8) as array size increases. The mean number of atom moves increases linearly while the extra moves ratio decays as the array size increases. The calculation of the ideal number of atom moves is demonstrated in the Supplementary Materials. Figure 3(d) shows that the average move distance per move increases linearly with the array side length.

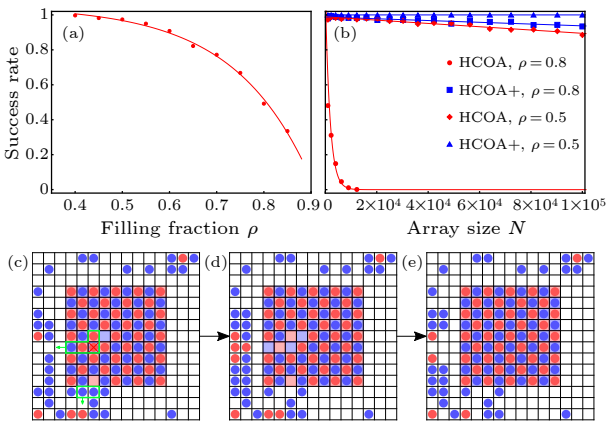

Fig. 4. Simulation result for HCOA and HCOA+ (HCOA+ is HCOA plus the complementary step) under high loading ratio ρ and scheme for the complementary step. (a) The success rate of HCOA vs loading ratio ($N=100$, zebra stripes pattern). (b) The success rate of HCOA and HCOA+ vs array size N under loading ratios 0.5 and 0.8. (c) A typical case that HCOA cannot solve. The atoms the complementary step decides to move are highlighted. The lower highlighted atoms are moved by the first and second steps while the upper highlighted atoms are moved by the third step. (d) The obstacle atoms are moved into outside empty sites. (e) The target region is properly filled using HCOA.

However, we find that HCOA is not good at rearranging with a high loading ratio. Taking the 10×10 zebra strip pattern as an example, Fig. 4(a) shows that the HCOA success rate decreases rapidly under a higher loading ratio because more unsolvable cases appear. After executing HCOA, a typical example of the unsolvable cases are shown in Fig. 4(c), which is a near full-filled atom array with a small number of empty sites. This is very similar to the case of atom loss during the rearrangement which is caused by the finite transfer efficiency and the collision with background gas. To solve this problem, we add following complementary steps. As the connected empty site region marked as *connected component*, we first find out one connected component which possesses at least one target empty site adjacent to the outside region. Second, we connect the found region with the nearest connected component through moving atoms blocking them. Third, we link the connected components which have outside empty sites with the misplaced atoms and connected components in the target region, through moving atoms [Figs. 4(c)–4(d)]. Finally, we execute the former four steps (HCOA) again [Fig. 4(e)]. The three procedures can loop for customized times to achieve a high success rate. Figure 4(b) shows the effectiveness of the complementary steps.

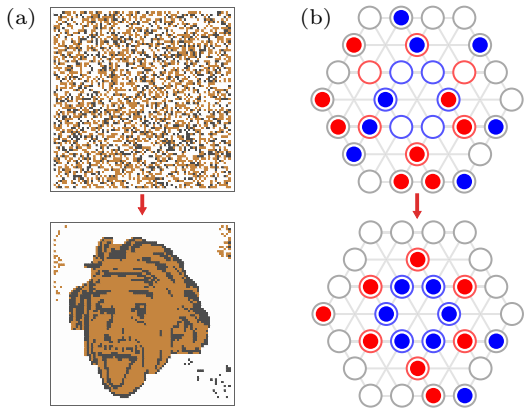

Fig. 5. Two rearrangement examples by HCOA from the stochastic initial configuration. (a) Einstein's portrait in 80×80 a square lattice, where each optical trap is represented by a square block and the square blocks with different colors represent atoms of different types, respectively. Atoms can only be transported between the adjacent optical traps. (b) Kagome lattice where straight lines indicate atoms can be transported between two traps connected by them.

In the end, we simulate the rearrangement of Einstein portrait in an 80×80 square lattice, an example in a kagome lattice in Fig. 5 to demonstrate the scalability of HCOA, which can be extended to rearrange almost all the atom configurations. The corresponding demonstration movies are uploaded to a web site https://github.com/YLG-WHU/Dual-species-atom-rearrangement-demonstration.

In summary, we have proposed a heuristic rearrangement algorithm for multi-species. The simulation results indicate that HCOA has a high success rate and fast speed for various multi-species target atom patterns and grid sizes ranging from 10×10 to 100×100. Compared with the former one in Ref. [19], whose algorithm decays exponentially, our algorithm shows a much higher success

rate (see the Supplementary Materials for the comparison diagram). Moreover, because our algorithm is based on the undirected graph, it can be easily extended to various optical trap configurations and transport ways defined by users. In the future, it is promised to control more mobile tweezers simultaneously for rearrangement in order to reduce the preparation time. Our algorithm can also be modified to adapt the many-optical-tweezer rearrangement by simultaneously considering several objects in the priority list using parallel computing or adjusting the move order of the final output move path.

Acknowledgments. This work was supported by the National Key R&D Program of China (Grant Nos. 2021YFA1402001 and 2017YFA0304501), the Youth Innovation Promotion Association, CAS (Grant Nos. Y2021091 and 2019325), the National Natural Science Foundation of China (Grant Nos. U20A2074 and 12074391), the K. C. Wong Education Foundation (Grant No. GJTD-2019-15).

References

[1] Wilk T, Gaëtan A, Evellin C, Wolters J, Miroshnychenko Y, Grangier P and Browaeys A 2010 *Phys. Rev. Lett.* **104** 010502
[2] Henriet L, Beguin L, Signoles A, Lahaye T, B, Reymond G O and Jurczak C 2020 *Quantum* **4** 327
[3] Saffman M 2019 *Natl. Sci. Rev.* **6** 24
[4] Saffman M, Walker T G and Mølmer K 2010 *Rev. Mod. Phys.* **82** 2313
[5] Xia T, Lichtman M, Maller K, Carr A, Piotrowicz M, Isenhower L and Saffman M 2015 *Phys. Rev. Lett.* **114** 100503
[6] Fu Z, Xu P, Sun Y, Liu Y, He X, Li X, Liu M, Li R, Wang J, Liu L and Zhan M S 2022 *Phys. Rev. A* **105** 042430
[7] Levine H, Keesling A, Semeghini G, Omran A, Wang T T, Ebadi S, Bernien H, Greiner M, Vuletić V, Pichler H and Lukin M D 2019 *Phys. Rev. Lett.* **123** 170503
[8] Wu T Y, Kumar A, Giraldo F and Weiss D S 2019 *Nat. Phys.* **15** 538
[9] Isenhower L, Urban E, Zhang X L, Gill A T, Henage T, Johnson T A, Walker T G and Saffman M 2010 *Phys. Rev. Lett.* **104** 010503
[10] Beterov I I and Saffman M 2015 *Phys. Rev. A* **92** 042710
[11] Belyansky R, Young J T, Bienias P, Eldredge Z, Kaufman A M, Zoller P and Gorshkov A V 2019 *Phys. Rev. Lett.* **123** 213603
[12] Auger J M, Bergamini S and Browne D E 2017 *Phys. Rev. A* **96** 052320
[13] Weimer H, Muller M, Lesanovsky I, Zoller P and Buchler H P 2010 *Nat. Phys.* **6** 382
[14] Browaeys A and Lahaye T 2020 *Nat. Phys.* **16** 132
[15] Liu L R, Hood J D, Yu Y, Zhang J T, Hutzler N R, Rosenband T and Ni K K 2018 *Science* **360** 900
[16] Liu L R, Hood J D, Yu Y, Zhang J T, Wang K, Lin Y W, Rosenband T and Ni K K 2019 *Phys. Rev. X* **9** 021039
[17] Zhang J T, Yu Y, Cairncross W B, Wang K, Picard L R B, Hood J D, Lin Y W, Hutson J M and Ni K K 2020 *Phys. Rev. Lett.* **124** 253401
[18] He X D, Wang K P, Zhuang J, Xu P, Gao X, Guo R J, Sheng C, Liu M, Wang J, Li J M, Shlyapnikov G V, Zhan M S 2020 *Science* **370** 331
[19] Sheng C, Hou J Y, He X D, Wang K P, Guo R J, Mamat B, Xu P, Lin M, Wang J and Zhan M S 2022 *Phys. Rev. Lett.* **128** 083202
[20] Lee W, Kim H and Ahn J 2017 *Phys. Rev. A* **95** 053424
[21] Sheng C, Hou J, He X, Xu P, Wang K, Zhuang J, Li X, Liu M, Wang J and Zhan M S 2021 *Phys. Rev. Res.* **3** 023008
[22] Schymik K N, Lienhard V, Barredo D, Scholl P, Williams H, Browaeys A and Lahaye T 2020 *Phys. Rev. A* **102** 063107
[23] Barredo D, Léséleuc S, Lienhard V, Lahaye T and Browaeys A 2016 *Science* **354** 1021
[24] Barredo D, Lienhard V, Léséleuc S, Lahaye T and Browaeys A 2018 *Nature* **561** 79
[25] Lee W, Kim H and Ahn J 2016 *Opt. Express* **24** 9816
[26] Kumar A, Wu T Y, Giraldo F and Weiss D S 2018 *Nature* **561** 83
[27] Endres M, Bernien H, Keesling A, Levine H, Anschuetz E R, Krajenbrink A, Senko C, Vuletic V, Greiner M and Lukin M D 2016 *Science* **354** 1024
[28] Singh K, Anand S, Pocklington A, Kemp J T and Bernien H 2022 *Phys. Rev. X* **12** 011040
[29] Zhang J T, Picard L R B, Carincross W B, Wang K, Yu Y, Fang F and Ni K K 2022 *Quantum Sci. Technol.* **7** 035006

Supplemental Materials: Efficient two-dimensional defect-free dual-species atom arrays rearrangement algorithm with near-fewest atom moves*

Zhi-Jin Tao(陶知进),[1,2,†] Li-Geng Yu(余立庚),[1,2,†] Peng-Xu(许鹏),[1,3,‡] Jia-Yi Hou(侯嘉毅),[1] Xiao-Dong He(何晓东),[1] and Ming-Sheng Zhan(詹明生)[1,3]

[1] *State Key Laboratory of Magnetic Resonance and Atomic and Molecular Physics, Wuhan Institute of Physics and Mathematics, Innovation Academy for Precision Measurement Science and Technology, Chinese Academy of Sciences, Wuhan 430071, China*

[2] *School of Physics and Technology, Wuhan University, Wuhan 430072, China*

[3] *Wuhan Institute of Quantum Technology, Wuhan 430206, China*

I. DETAILED STEPS

The general algorithm structure of each step can be summarized as a loop structure (Fig.1). The loop body can be characterized as two steps: Firstly, get the list of objects needed to be processed, e.g., misplaced atoms, obstacle atoms, or empty sites, sorted by particular priority; Secondly, find ways to process the object at first of the list. If the object has no feasible way to handle, try the next one. Otherwise, delete the object in the list and try the next one. If the next one is none, determine whether the loop should be terminated. The loop terminates when the list is empty, or all the objects fail to be processed. Otherwise, continue the next loop. The following is a general explanation of each step:

The first step aims to move the misplaced atoms to the target empty sites or outside sites. We made the following considerations to improve the connectivity of the empty site graph during each move. First, get the list of misplaced atoms. Optionally, sort the list by atom partition number. Second, find the empty site s with partition number 0 which the atom can reach [Fig.2.(a,b)]. To approach the fewest atom moves, a misplaced atom is preferentially moved to a target empty site, and the target region mustn't form a new misplaced atom or a new blocked misplaced atom after each move [Fig.2.(c)]. Fig.2 demonstrates how step1 is carried out. In this example, all the misplaced atoms are removed. The connected components of the graph of the empty site have reached a lower level, which provides a good condition for the execution of the following steps.

Step 2 removes the misplaced atoms unsolved by step 1 and eliminates the enclosed target empty sites region. If one algorithm ignores these cases, the success rate will drop catastrophically. Before illustration of step 2, we introduce the first-layer obstacle atom and block number concept. The first layer obstacle atom blocking misplaced atoms are the atom whose adjacent empty sites or the atoms itself can be reached by the misplaced atoms. The block number is the number of misplaced atoms the obstacle atom blocks. The scheme of the first layer obstacle atom and block number is shown in Fig.4.

First, we get the list of first-layer obstacle atoms and sort them by block number. The first-layer obstacle atom with a greater block number is moved to a higher priority. Fig.3. (a) shows the first-layer obstacle atoms

* Supported by the National Key R&D Program of China (Grant No. 2021YFA1402001, No. 2017YFA0304501), the Youth Innovation Promotion Association CAS No. Y2021091 and No. 2019325, the National Natural Science Foundation of China under Grant No. U20A2074 and No. 12074391, the K.C. Wong Education Foundation (Grant No. GJTD-2019-15)

† Z.T. and L.Y contributed equally to this work.

‡ xupeng@apm.ac.cn

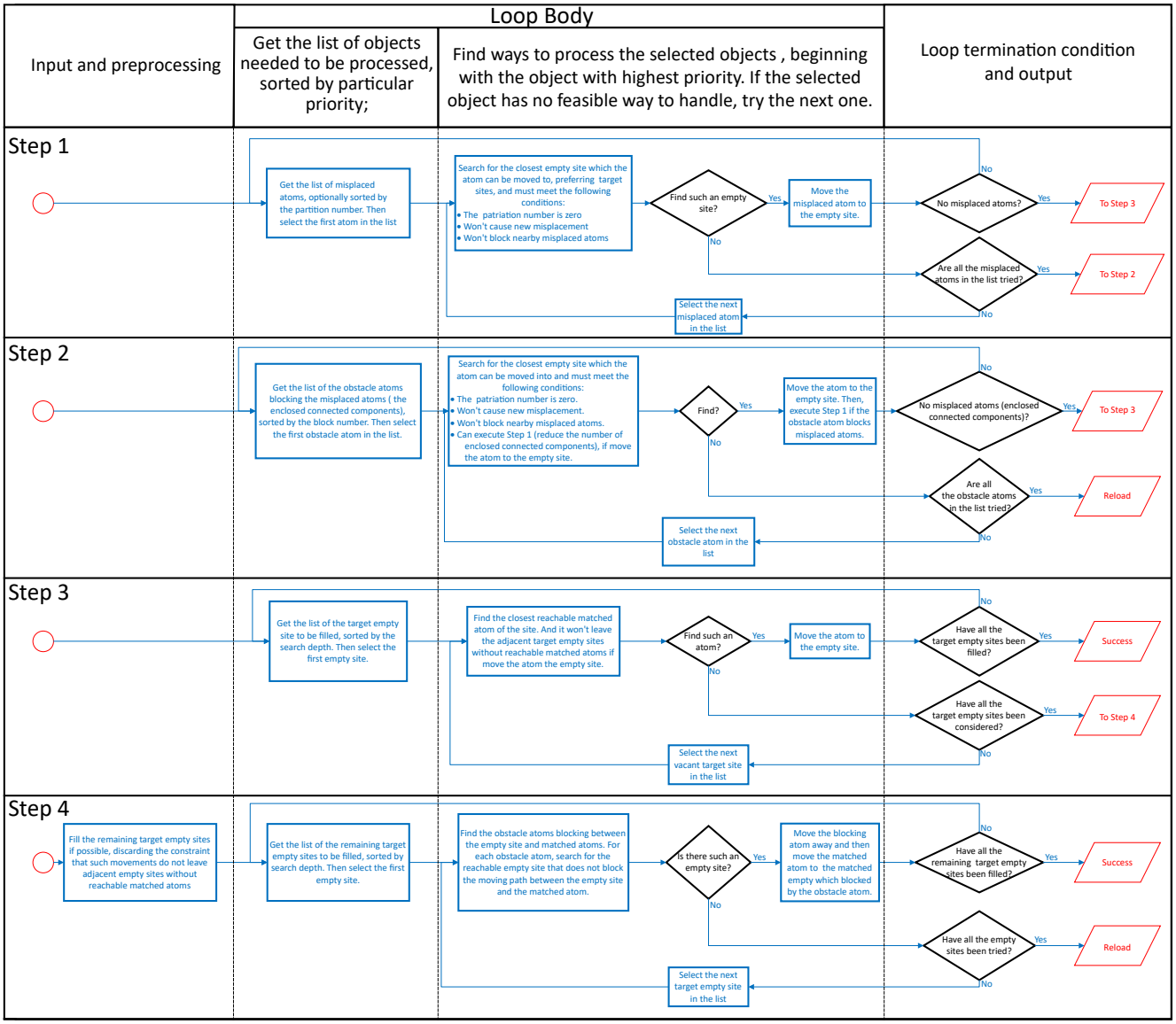

Fig.1 Detailed flowchart for each step

blocking misplaced atoms, labeled by their block number. Move the obstacle atom to the empty site that meets the following conditions: won't cause new misplacement or block adjacent misplaced atoms after the move. The partition number of the empty site is 0 when treating the atom to be moved as an empty site. If such an empty site exists, move the atom to the empty site, execute step 1, and process the next first-layer obstacle atom. Otherwise, process the next first-layer obstacle atom with lower priority. When all the misplaced atoms are moved to the matched empty sites, move the boundary atoms of the enclosed target empty sites region to the empty sites that satisfy the former three conditions until there is no enclosed target empty region. Fig.3. (b) demonstrates the moving atoms and move paths of step 2. The probability of executing step 2 is shown in Fig.3.(d). After the step 2, all the target empty sites regions are connected with the outside region, which brings convenience for the step 3.

Step 3 is to fill target empty sites. As target empty sites s generally have positive partition number

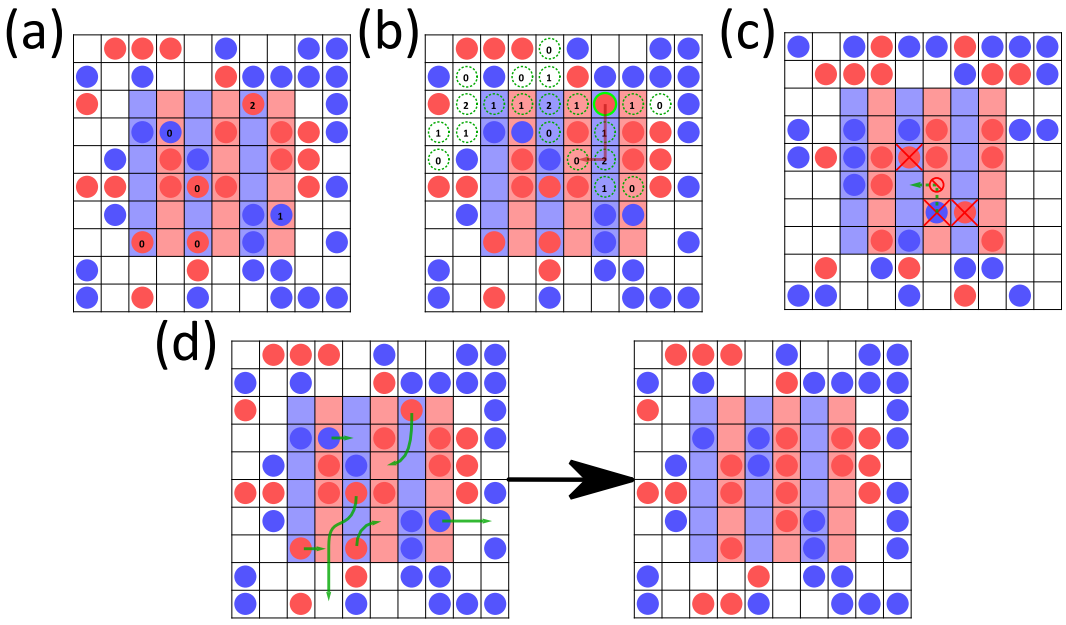

Fig.2 Schemes of step 1. (a) The initial atom array of the example. Misplaced atoms are labeled by their partition numbers. (b) The first move in executing step 1 for the initial atom array. The circled atom is selected to be moved firstly because it has the biggest partition number. Empty sites reached by the selected atom are marked by the dotted circle and labeled by their partition number. Step 1 decides to move the selected atom along the arrow, as the empty destination site is the closest matched empty site with zero partition number. (c) An example that a move will block the adjacent misplaced atoms. (d) Move paths of misplaced atoms in step 1 and the configuration of the atom array after executing step 1.

$P(G, s) > 0$ in this stage, we changed the heuristic strategy: preferentially fill the empty target site deeper to the boundary of the target region. The method to determine the depth of an empty site to the boundary of target region is shown in Fig.5.(a). A move in the filling process is to move the closest matched atom outside to the empty target site. To improve the success rate of step 3, such a move in the filling process shouldn't leave adjacent target sites having any reachable matched atoms in the outside region (An example is shown in Fig.5.(c)).

To solve the cases left unsolved by step 3, we introduced step 4. Fig.6.(b) shows the probability of executing step 4 decreases with the grid size increasing, demonstrating the former 3 steps are almost enough for the larger grid size. The preprocessing step of step 4 is filling the target empty sites by matched atoms in the outside region, ignoring the restriction that such a move will not leave adjacent target sites has no reachable matched atom in the outside region in step 3, and add a restriction that such a move will not form any enclosed empty sites in the target region (see Fig.6.(b)) Then find out the obstacle atoms blocking the shortest moving path of an atom in the outside region to the matched empty target site. Move one obstacle atom to empty sites not blocking the moving path if possible, and then fill the empty target site by the matched atom through the shortest moving path (see Fig.6.(c)).

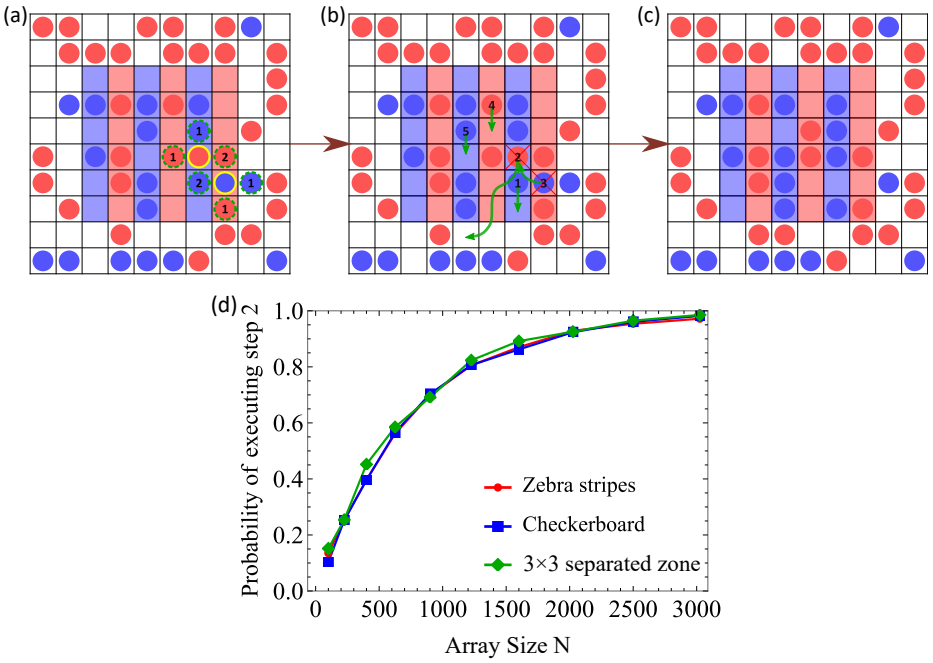

Fig.3 Scheme of step 2. (a) The dotted and circled atoms represent the obstacle atoms, labeled by their block numbers. The atoms circled with yellow lines are misplaced atoms. (b) Move paths of step 2 for this example. (c) The atom array configuration after executing step 2. (d) The probability of executing step 2.

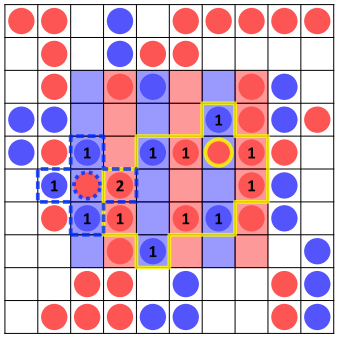

Fig.4 Scheme of the first layer obstacle atom and block number.The first layer obstacle atoms for each misplaced atom circled with solid (dashed) line are framed with solid (dashed) line. The misplaced atom circled by dashed line has no empty site to move into, while the misplaced atom circled by solid line has no empty site satisfying conditions required in step 1 to move into. The first layer obstacle atoms are labeled by their block number.

II. THE DEMONSTRATION PROGRAM

The demonstration program for HCOA is uploaded to Github:

https://github.com/YLG-WHU/Dual-species-atom-rearrangement-demonstration.

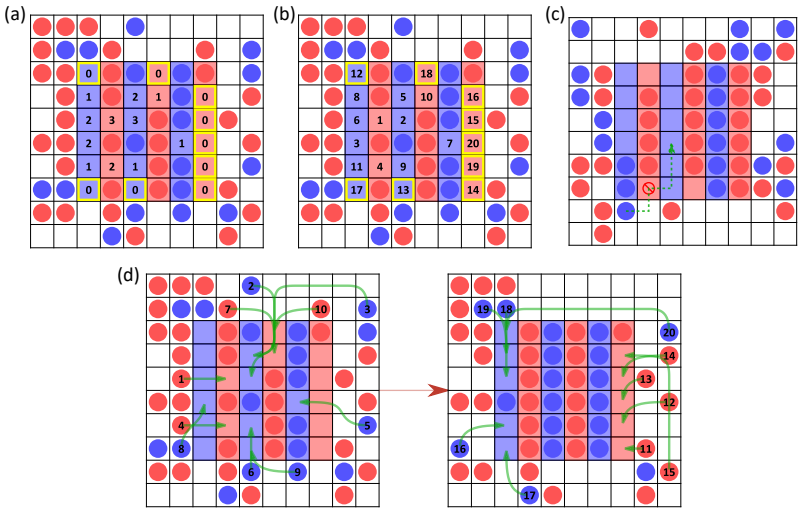

Fig.5 Scheme of step 3. (a) Method to determine depth to the boundary of target region. First, find the empty target sites with zero depth, which are neighbor to the boundary and their adjacent sites in outside region are not all unmatched atoms. The zero depth sites are framed. Second, do the broad first search, beginning with the zero depth sites until all empty target sites are labeled by their depth to the boundary of target region. (b) The priority level of empty target sites. The empty target site deeper to the boundary and having less neighbor empty sites is prior to be filled. (c) An example of such a move which leaves the adjacent target sites having no reachable matched atom in the outside region. (d) An example of executing step 3. All empty target sites are filled. The moved atoms are labeled by their move orders.

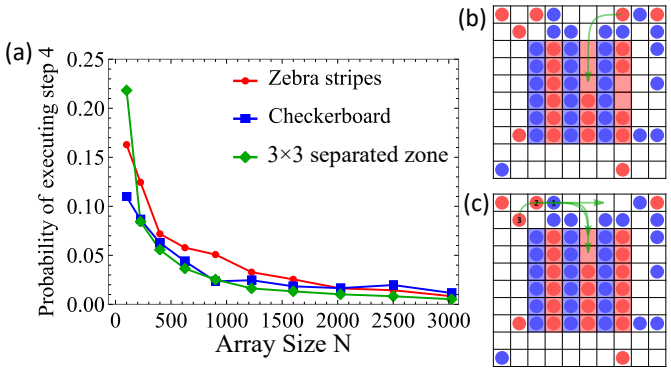

Fig.6 Scheme of step 4. (a) Probability of executing step 4 for three different target site patterns vs grid size. (b) The preprocessing step of step 4. Fill the remaining target empty sites if possible, discarding the constraint that such movements do not leave adjacent empty sites without reachable matched atoms. (c) An example of step 4: the obstacle atom labeled by 1 is moved away, and then the remaining target empty sites are filled by matched atoms labeled by 2 and 3

III. THE IDEAL ATOM MOVES

The ideal number of atom moves M_m is defined as the minimum number of atom moves needed to rearrange the initially loaded atoms to the target configuration if any atom can be directly moved to any site. After loading

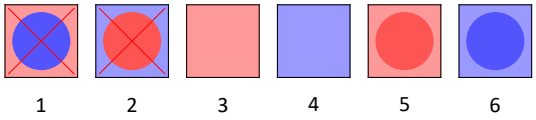

Fig.7 The six types of site-atom patterns

the atoms stochastically, there are six types of site-atom patterns [see in Fig.7]. The type-1 pattern and type-2 pattern refer to the sites filled with misplaced atoms. The type-3 pattern and type-4 pattern represent the empty sites. The type-5 pattern and type-6 pattern are the sites filled with the matched atoms. Then $N_m = max(N_1, N_2 + N_4) + max(N_2, N_1 + N_3)$, where $N_i, i = 1..6$ is the number of each pattern.

The target blue and red sites should be filled with the matched atoms, so we first move the misplaced atoms to such target sites. Obviously, the misplaced atoms are eliminated in the first step if $N_1 \leq N_2 + N_4$ and $N_2 \leq N_1 + N_3$. In this way, then move the outside atoms to the matched empty sites, and the minimum number of atom moves is $N_2 + N_4 + N_1 + N_3$. It should be noted that the type-2 site and type-1 site is allowed to be filled with the matched atom and the misplaced atom simultaneously if the misplaced blue atoms or red atoms are more than the sites not filled with the matched atoms, i.e., $N_1 > N_2 + N_4$ or $N_2 > N_1 + N_3$. In this case, the target sites are filled with the matched atoms, and some of the target sites are filled with two different atoms; then, move the extra misplaced atoms to the empty outside site, and the target configuration is achieved. So $N_m = max(N_1, N_2 + N_4) + max(N_2, N_1 + N_3)$.

IV. COMPARISON OF THE SUCCESS RATE BETWEEN HCOA AND HHA

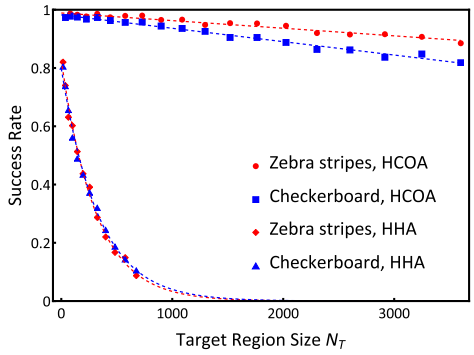

Fig.8 The comparison of success rate between HCOA and HHA. The success rate of HHA algorithm is fitted with an exponential decay function $y = a \times 10^{-bx}$, for Zebra strips pattern $a = 0.83 \pm 0.03$, $b = -0.00140 \pm 0.00004$ and for Checkerboard pattern $a = 0.80 \pm 0.01$, $b = -0.00130 \pm 0.00003$; The success rate of HCOA algorithm is fitted with a linear curve $y = a + bx$, for Zebra strips pattern $a = 0.989 \pm 0.003$, $b = (2.6 \pm 0.2) \times 10^{-5}$ and for Checkerboard pattern $a = 0.982 \pm 0.003$, $b = (4.6 \pm 0.1) \times 10^{-5}$.

Fig.8 shows the comparison of the success rate between HCOA and HHA. From the graph, HCOA shows a much higher success rate compared with HHA and remains at a high level with the target region size increasing. By taking the connectivity of the graph as a critical consideration at the main steps, the success rate of HCOA decreases linearly with the number of atoms increasing and remains larger than 0.80 as the number of target

atoms increase to 3600.

V. ANALYSIS FOR THE EFFECTIVENESS OF CONNECTIVITY

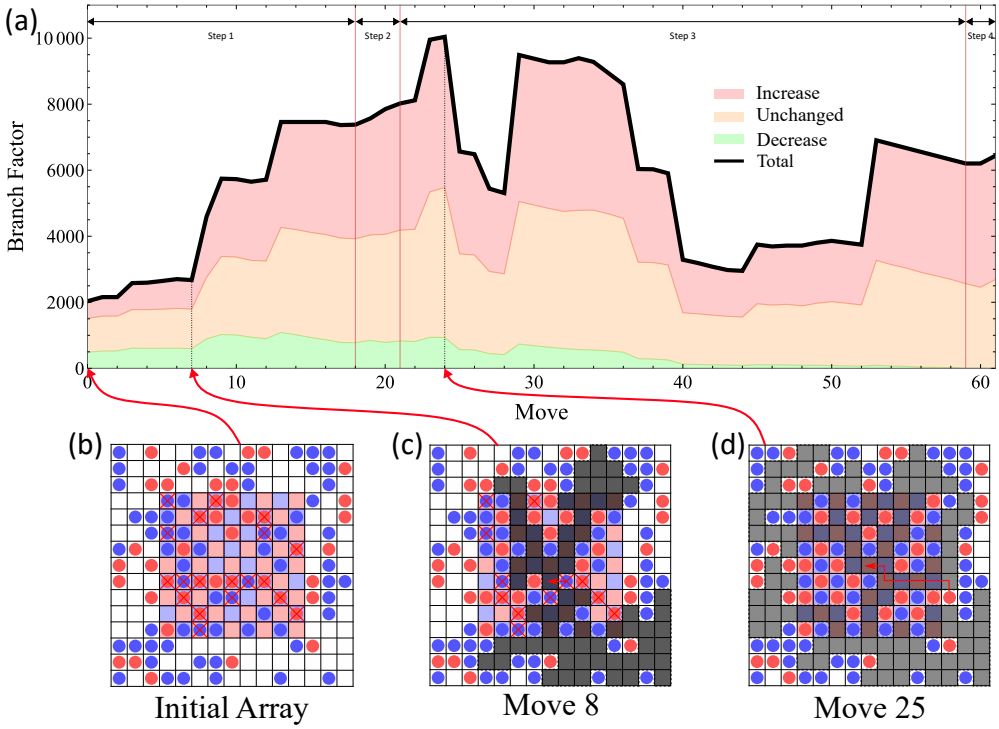

Fig.9 Branch factor vs moves for an example of 15 × 15 square atom array rearrangement. (a) Total possible atom move paths(branch factor) vs moves in one rearrangement process.The pink, orange, green regions represent the possible atom move paths which will increase, unchange, decrease the total atom configuration entropy respectively (C. Sheng *et al.*'s work[1] provides calculation formula for atom array configuration entropy). (b) The initial array configuration. (c) Atom array configuration in Move 8. The branch factor increases significantly due to the misplaced atom separating two large connected components (colored dark) being removed. (d) Atom array configuration in Move 25. The branch factor reaches maximum with the connected components number dropping a lot and thus connectivity of the graph improves a lot.

Fig.9 shows the branching factor(the total possible atom move paths) vs. rearrangement steps in our algorithm. Fig.9 suggests that the branching factor maximizes when the empty sites are nearly connected, which proves the importance of the graph's connectivity.

REFERENCES

[1] C. Sheng, J.-Y. Hou, X.-D. He, K.-P. Wang, R.-J.Guo, B. Mamat, P. Xu, M. Lin, J. Wang and M.-S. Zhan. 2022 *Physical Review Letters* **128** 083202